Research Article

Rajesh Raju*, Raghavachary Raghunathan, Natarajan Arumugam*, Abdulrahman I. Almansour, Raju Suresh Kumar, P. A. Vivekanand, Cheriyan Ebenezer, Rajadurai Vijay Solomon, and Karthikeyan Perumal

Environmentally friendly synthesis and computational studies of novel class of acridinedione integrated spirothiopyrrolizidines/indolizidines

https://doi.org/10.1515/gps-2023-0036
received March 01, 2023; accepted June 18, 2023

Abstract: An efficient and environmentally benign synthesis of a new class of acridinedione embedded spirooxindolo/acenaphthenothiopyrrolizidines and spirooxindolo/acenathenoindolizidines has been synthesized in good to excellent yields employing ionic liquid accelerated one-pot [3 + 2]-cycloaddition strategy. The pre-requisite starting substrates, *O*-acryloyl acridinediones were prepared from dimedone in three good yielding steps, while the 1,3-dipole was derived *in situ* from isatin/acenaphthenequinone and thiazolidine-4-carboxylc acid/L-pipecolinic acid via decarboxylative condensation. The cycloadduct possesses three stereogenic carbons, one of which is a spiro carbon through the formation of two C–C and one C–N bonds in one-pot synthetic transformation. Geometrical parameters of the synthesized compounds were calculated using the B3LYP/6-311g(d,p) level of theory. The activity of these molecules was evaluated against main protease of COVID-19 to screen them for their inhibitor efficiency. In order to get a broad understanding of the interactions of these synthesized ligands, a detailed molecular docking analysis was performed. Molecular docking analysis shows that compound **8b** has the highest binding affinity toward the protein. The compound can be a potential candidate for the treatment of COVID-19.

Keywords: spirooxindolo/acenathenothiopyrrolidines, spirooxindolo/acenathenoindolizidines, acridinedione, ecofriendly green protocol, 1,3-dipolar cycloaddition

1 Introduction

Hybrid heterocycles play an essential role in drug discovery because of their presence in a significant number of drugs [1]. Heterocycles not only provide protein-binding functional groups, but also have a beneficial effect on drug solubility and its pharmacokinetic properties. Spiro compound-embedded heterocycles have emerged as particularly attractive synthetic targets in drug discovery because of their structural rigidity and inherent structural complexity and ability to expose functionality that offers enhanced affinity to biotargets [2]. In addition, the spiro compounds serve as useful molecular scaffolds for exploring and utilizing the pharmacophore space, which has led to the discovery of new drug leads. Spiro compounds containing acenaphthenone or oxindole moieties are of particular interest in medicinal chemistry because of their interesting biological properties, including antimicrobial, cholinesterase inhibitory activity, anticancer, and anti-mycobaterium tuberculosis activities [3–10]. Similarly, thiazolidine and indolizidine, an important class of heterocyclic motifs found in many naturally occurring alkaloids, has displayed a wide range of biological activities [11–14].

*** Corresponding author: Rajesh Raju**, Department of Organic Chemistry, University of Madras, Guindy Campus, Chennai 600 025, India, e-mail: vrajurajesh@gmail.com
*** Corresponding author: Natarajan Arumugam,** Department of Chemistry, College of Science, King Saud University, P.O. Box 2455, Riyadh 11451, Saudi Arabia, e-mail: anatarajan@ksu.edu.sa
Raghavachary Raghunathan: Department of Organic Chemistry, University of Madras, Guindy Campus, Chennai 600 025, India
Abdulrahman I. Almansour, **Raju Suresh Kumar:** Department of Chemistry, College of Science, King Saud University, P.O. Box 2455, Riyadh 11451, Saudi Arabia
P. A. Vivekanand: Centre for Catalysis Research and Department of Chemistry, Saveetha Engineering College, Chennai 602 105, Tamil Nadu, India
Cheriyan Ebenezer, **Rajadurai Vijay Solomon:** Department of Chemistry, Madras Christian College (Autonomous) (Affiliated to the University of Madras), Chennai 600 059, Tamil Nadu, India
Karthikeyan Perumal: Department of Chemistry and Biochemistry, The Ohio State University, 151 W. Woodruff Ave, Columbus, OH 43210, USA

Among the typical synthetic transformations leading to the spiroheterocyclic hybrids, multicomponent 1,3-dipolar cycloaddition of electron-deficient exocyclic alkenes with 1,3-dipole, derived from non-enolizable diketones and α-amino acids, is the most widely accepted synthetic strategy [15–19] as it allows the creation of several bonds in one-pot synthetic transformation that led to facilitate exciting advantages such as (i) direct isolation of target product, (ii) minimal number of synthetic operation which in turn minimize the waste, (iii) atom economy and ease automization, and (iv) operational simplicity. In addition, this strategy aids the effective generation of a series of potent pharmaceutically stimulating drug like compounds and plays an essential role in combinatorial and diversity-oriented synthesis [20]. Incidentally, it is known that the acridine structural motif possesses multifarious biological activities [22–24] and is an active motif present in numerous alkaloids [25].

Recently, we have reported a series of acridinedione bridged hybrid spiroheterocycles employing cascade cycloaddition reaction process via decarboxylative condensation [21]. In continuation of our research in the cycloaddition process and the biological importance of the above spiro compounds encouraged us to attempt the preparation of series of structurally interesting new classes of heterocycles embedding acridinedione and spirooxindole/acenapthenothiopyrrolizidines/indolizidines employing single pot cycloaddition strategy. In our earlier study, we reported the synthesis of spiropyrrolidine/pyrrolizidines derived from *N*-methylglycine and L-proline by 1,3-dipolarcycloaddition strategy [21]. In the present investigation, herein we report the synthesis and computational studies of a structurally intriguing new class of acridinedione tethered spirooxindolothiopyrrolizidines/indolizidines and acenaphthenothiopyrrolizidines/indolizidines derived from thiazolidine-4-carboxylc acid/pipecolinic acid employing ionic liquid-assisted intermolecular cycloaddition cascade green reaction sequence. Furthermore, *O*-acryloyl acridinediones utilized as dipolarophile for cycloaddition reaction is relatively less explored in the literature. The reaction sequence has been described in the flow chart of Figure 1a and the synthetic approach for the preparation of spiro compounds from amino acids and α,ά-diketones as outlined in Figure 1b. It is important to note that new structural novelty and diversity will lead to the addition of some better biological activities that are of paramount importance in medicinal chemistry. On the other hand, computational methods have unlocked new ways in understanding the chemical properties of molecules using calculations as a substitute for experimental investigation. The computational approach is not laborious and can be achieved effortlessly. The recent effects of density functional theory (DFT) methods together with quantum chemical calculations are significant. As DFT is great in predicting the chemical and physical properties of molecules with great accuracy, it is one among the most effective and useful computational tools [26,27].

2 Materials and methods

2.1 General procedure for the synthesis of *O*-acryloylacridinedione dipolarophile, 5a–b

To a solution of acridinedione **4a–b** (1.0 g, 2.6 mmol) in dry dichloromethane (DCM) (40 mL) kept at 0–5°C triethylamine was added (1 mL) followed by acryloyl chloride (0.24 g, 2.6 mmol). Then the reaction mixture was stirred at RT for 5 h and after completion of the reaction, as monitored by thin layer chromatography (TLC), the triethylamine hydrochloride was filtered off. Upon concentrating the filtrate under reduced pressure below 50°C, a viscous material was obtained. The viscous material was dissolved in DCM and made into a slurry with silica gel. Column chromatography over silica gel with 2% methanol in chloroform as eluent furnished the compound **5a–b**.

2.1.1 4-(3,3,6,6-Tetramethyl-9-phenyl-3,4,6,7,9,10-hexahydro-1,8(2*H*,5*H*)acridinedione-10-yl)phenyl acrylate (5a)

Yield: 75%. Yellow solid, mp 210–212°C; ^{1}H NMR ($CDCl_3$, 300 MHz): δ 0.81 (s, 6H), 0.96 (s, 6H), 1.82–1.88 (d, 2H, J = 17.4 Hz), 2.15–2.18 (d, 4H, J = 7.8 Hz), 5.27 (s, 1H), 6.10–6.13 (d, 1H, J = 10.2 Hz), 6.33–6.42 (dd, 1H, J = 10.5 Hz), 6.66–6.71 (d, 1H, J = 17.4 Hz), 7.08–7.43 (m, 9H). ^{13}C NMR ($CDCl_3$, 75 MHz): δ 26.77, 29.73, 32.42, 41.83, 50.22, 114.77, 123.17, 125.98, 127.44, 127.83, 128.08, 133.62, 136.35, 146.02, 149.66, 150.91, 163.95, 195.80. Mass: m/z 495 (M^+). Anal. calculated for $C_{32}H_{33}NO_4$: C, 77.55%; H, 6.71%; N, 2.83%; Found: C, 77.66%; H, 6.80%; N, 2.96%.

2.1.2 4-(3,3,6,6,-Tetramethyl-9-(4-nitrophenyl)-3,4,7,9,10-hexahydro-1,8(2*H*,8*H*) acridinedione-10-yl) phenylacrylate (5b)

Yield: 79%. Yellow solid, mp 210–212°C; ^{1}H NMR ($CDCl_3$, 300 MHz): δ 0.81 (s, 6H), 1.12 (s, 6H), 1.84–1.90 (d, 4H, J = 17.4 Hz), 2.08–2.13 (d, 2H, J = 16.8 Hz), 2.17–2.19 (d, 4H, J = 6.0 Hz), 5.34 (m, 1H), 6.10–6.14 (d, 1H, J = 10.5 Hz), 66.33–6.42

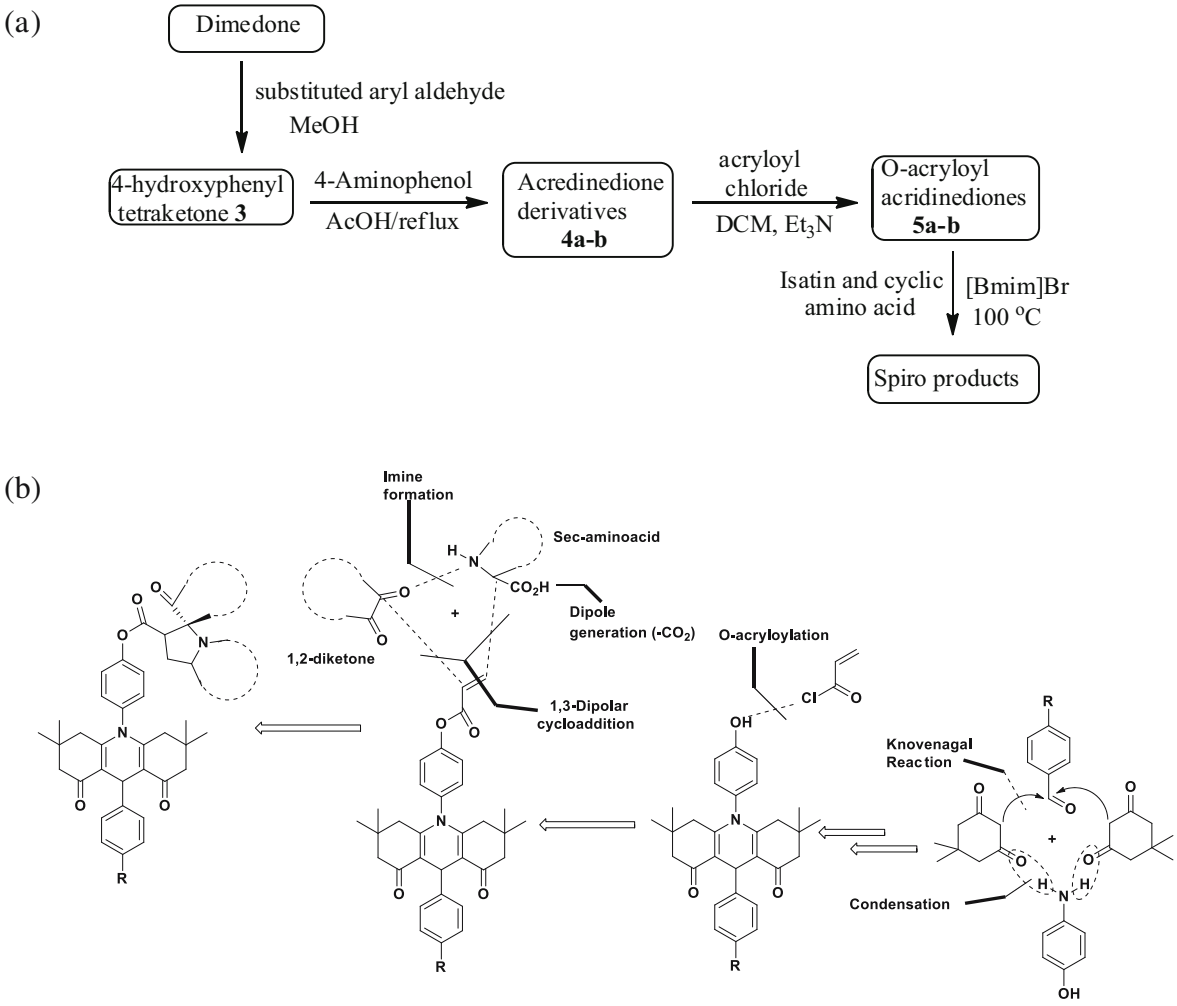

Figure 1: (a) Flow chart for synthesis of spirocycloadducts and (b) synthetic approaches for acridinedione tethered spiro heterocyclic analogs.

(dd, 1H, J = 10.2, 10.5 Hz), 6.6–6.72 (d, 1H, J = 10.8 Hz), 7.25–7.28 (m, 3H), 7.39–7.61 (m, 3H), 8.07–8.14 (m, 2H). ^{13}C NMR ($CDCl_3$, 75 MHz):δ 26.75, 29.23, 32.23, 40.84, 41.90, 50.04, 113.75, 114.54, 123.43, 127.38, 128.84, 129.36, 133.73, 135.94, 146.24, 150.27, 151.12, 153.44, 162.90, 195.64, 196.26. Mass: m/z 540 (M^+). Anal. calculated for $C_{32}H_{32}N_2O_6$: C, 71.09%; H, 5.97%; N, 5.18%; Found: C, 71.20%; H, 6.07%; N, 5.27%.

2.2 General procedure for the synthesis of cycloadducts

A mixture of *O*-acryloylacridinedione dipolarophile **5a–b** (1 mmol), thiazolidine-4-carboxylc acid **7/**pipecolinic acid **9** (1 mmol) and isatin **6**/acenapthenequinone (**11**) (1 mmol) were heated in [Bmim]Br (3 mL) for 1 h at 100°C. After completion of reaction (TLC), the reaction mixture was diluted with EtOAc (2 × 5 mL). The ethyl acetate layer was extracted and reduced under low temperature. The crude compounds were separated by column chromatography with chloroform–methanol (9:1) mixture to get the cycloadducts in good yields.

2.2.1 Spiro[2.3′]-oxindolo-3-[4″-(3,3,6,6-tetramethyl-9-phenyl-3,4,6,7,9,10-hexahydro-1,8(2*H*,5*H*) acridinedione-10-yl)phenyl]carboxylate thiopyrrolizidine (8a)

Yield: 92%. Yellow solid, mp 210–212°C;^{1}H NMR ($CDCl_3$, 300 MHz): δ 0.77 (s, 6H), 0.92 (s, 6H), 1.69–1.75 (d, 2H, J = 18.3 Hz), 1.94–2.00 (d, 2H, J = 17.4 Hz), 2.13–2.15 (d, 4H, J = 6.0 Hz), 2.32–2.44 (m, 1H), 2.54–2.62 (m, 1H), 3.01–3.05 (d, 1H, J = 11.7 Hz), 3.18–3.25 (m, 1H), 3.48–3.52 (d, 1H, J = 10.8 Hz), 3.90–3.93 (d, 1H, J = 10.8 Hz), 3.97–4.03 (dd, 1H, J = 6.6, 6.9 Hz), 4.34–4.37 (m, 1H), 5.24 (s, 1H), 6.40–6.43 (d, 2H, J = 8.4 Hz), 7.00–7.16 (m, 4H), 718–7.23 (m, 3H), 7.35–7.43 (m, 3H), 7.60–7.63 (d, 1H, J = 7.2 Hz), 9.05 (s, 1H). ^{13}C NMR

($CDCl_3$, 75 MHz): δ 26.74, 26.79, 29.67, 32.41, 32.56, 33.46, 38.17, 41.73, 50.14, 53.27, 54.97, 68.00, 73.97, 110.73, 114.72, 122.38, 122.89, 123.96, 126.03, 127.59, 127.78, 128.08, 130.45, 136.51, 142.23, 145.89, 149.79, 150.29, 168.44, 180.20, 196.08. Mass: *m*/*z* 713 (M^+). Anal. calculated for $C_{43}H_{43}N_3O_5S$: C, 72.35%; H, 6.07%; N, 5.89%; Found: C, 72.44%; H, 6.18%; N, 5.96%.

2.2.2 Spiro[2.3′]-oxindolo-3-[4″-(3,3,6,6-tetramethyl-9-(4-nitrophenyl)-3,4,6,7,9,10-hexahydro-1,8(2*H*,5*H*) acridinedione-10-yl)phenyl]carboxylate thiopyrrolizidine (8b)

Yield: 87%. Yellow solid, mp 210–212°C; ^{1}H NMR ($CDCl_3$, 300 MHz): δ 0.783 (s, 6H), 0.961 (s, 6H), 1.74–1.80 (d, 2H, *J* = 17.4 Hz), 2.16–2.10 (d, 2H, *J* = 18.6 Hz), 2.03 (s, 4H), 2.30–2.41 (m, 1H), 3.18–3.24 (m, 1H), 3.48–3.52 (d, 1H, *J* = 10.8 Hz), 3.89–3.93 (d, 1H, *J* = 10.8 Hz), 3.96–4.00 (dd, 1H, *J* = 7.2 Hz), 4.07–4.14 (dd, 2H, *J* = 6.9 Hz), 4.32–4.34 (m, 1H), 5.26 (s, 1H), 6.45–6.47(d, 2H, *J* = 8.2 Hz), 7.00–6.97 (d, 1H, *J* = 7.8 Hz), 7.07–7.10 (m, 2H), 7.33–7.38 (t, 1H, *J* = 8.1, 7.8 Hz), 7.53 (m, 3H), 8.03 (s, 1H), 8.08–8.11 (d, 2H, *J* = 8.4 Hz), 10.38 (s, 1H). ^{13}C NMR ($CDCl_3$, 75 MHz): δ 31.41, 34.30, 36.11, 38.18, 42.92, 46.37, 54.70, 57.85, 65.01, 72.65, 78.35, 115.20, 118.04, 126.42, 128.10, 128.68, 132.08, 133.55, 134.97, 140.58, 147.87, 150.81, 155.20, 155.31, 158.26, 167.27, 200.43, 184.10, 173.27. Mass: *m*/*z* 758 (M^+). Anal. calculated for $C_{43}H_{42}N_4O_7S$: C, 68.06%; H, 5.58%; N, 7.38%; Found: C, 68.15%; H, 5.65%; N, 7.49%.

2.2.3 Spiro[2.2′]-oxindolo-3-[4″-(3,3,6,6-tetramethyl-9-phenyl-3,4,6,7,9,10-hexahydro-1,8 (2*H*,5*H*) acridinedione-10-yl)phenyl]carboxylate indolizidine (10a)

Yield: 79%. Yellow solid, mp 210–212°C; ^{1}H NMR ($CDCl_3$, 300 MHz): δ 0.78 (s, 6H), 0.92 (s, 6H), 0.82 (m, 2H), 0.97 (m, 2H), 1.28–1.31 (m, 2H), 1.54–2.21 (m, 6H), 2.31–2.15 (d, 4H, *J* = 6.6 Hz), 2.29–2.50 (m, 2H), 3.26 (m, 1H), 3.69–3.76 (dd, 1H, *J* = 7.8 Hz), 5.24 (s, 1H), 6.45–6.43 (d, 2H, *J* = 6.0 Hz), 6.88–6.90 (d, 1H, *J* = 7.8 Hz), 7.01–7.04 (d, 2H, *J* = 9.0 Hz), 7.08–7.13 (m, 2H), 7.19–7.24 (t, 2H, *J* = 7.2, 7.8 Hz), 7.29–7.32 (m, 2H), 7.36–7.41 (m, 2H), 8.00 (s, 1H). ^{13}C NMR ($CDCl_3$, 75 MHz): δ 23.65, 25.64, 26.69, 29.56, 31.85, 32.85, 32.39, 33.49, 34.17, 41.71, 45.42, 49.95, 50.97, 59.49, 72.38, 109.58, 113.60, 122.94, 123.42, 126.01, 128.73, 129.01, 129.23, 129.48, 130.55, 135.80, 141.93, 146.12, 150.40, 150.54, 153.32, 170.09, 180.21, 195.79. Mass: *m*/*z* 709 (M^+). Anal. calculated for $C_{45}H_{47}N_3O_5$: C, 76.14%; H, 6.67%; N, 5.92%; Found: C, 76.25%; H, 6.76%; N, 5.98%.

2.2.4 Spiro[2.3′]-oxindolo-3-[4″-(3,3,6,6-tetramethyl-9-(4-nitrophenyl)-3,4,6,7,9,10-hexahydro-1,8(2*H*,5*H*) acridinedione)phenyl]carboxylate indolizidine (10b)

Yield: 81%. Yellow solid, mp 210–212°C; ^{1}H NMR ($CDCl_3$, 300 MHz): δ 0.77 (s, 6H), 0.94 (s, 6H), 0.82–0.85 (m, 2H), 0.98–1.01 (m, 2H), 1.31–1.35 (m, 2H), 1.71–2.21 (m, 6H), 2.12–2.16 (d, 4H), 2.30–2.53 (m, 2H), 3.22–3.33 (m, 1H), 3.70–3.76 (dd, 1H, *J* = 8.1, 7.5 Hz), 5.31 (s, 1H), 6.46–6.49(d, 2H, 8.2 Hz), 6.87–6.90 (d, 1H, *J* = 7.8 Hz), 7.02–7.04 (d, 2H, *J* = 8.4 Hz), 7.08–7.13 (t, 1H, *J* = 7.2, 7.5 Hz), 7.30–7.35 (m, 2H), 7.53–7.61 (m, 3H), 7.78 (s, 1H), 8.09–8.12 (d, 2H, *J* = 8.4 Hz).^{13}C NMR ($CDCl_3$, 75 MHz): δ 23.72, 25.69, 26.74, 29.59, 31.89, 32.44, 33.54, 34.22, 41.77, 45.48, 49.98, 51.06, 59.53, 72.44, 109.62, 113.64, 122.95, 123.49, 126.00, 128.8, 129.34, 129.50, 130.61, 135.89, 141.96, 146.20, 150.44, 150.66, 153.40, 170.10, 180.26, 195.84. Mass: *m*/*z* 754 (M^+). Anal. calculated for $C_{45}H_{46}N_4O_7$: C, 71.60%; H, 6.14%; N, 7.42%; Found: C, 71.72%; H, 6.26%; N, 7.54%.

2.2.5 Spiro[2.2′]-acenapthene-1′-one-3-[4″-(3,3,6,6-tetramethyl-9-phenyl-3,4,6,7,9,10-hexahydro-1,8(2*H*,5*H*)acridinedione-10-yl)phenyl]carboxylate thiopyrrolizidine (12a)

Yield: 80%. Yellow solid, mp 210–212°C; ^{1}H NMR ($CDCl_3$, 300 MHz): δ 0.73 (s, 6H), 0.88 (s, 6H), 1.52–1.59 (dd, 2H, *J* = 4.8 Hz), 1.80–1.87 (dd, 2H, *J* = 1.8, 2.1 Hz), 2.09–2.11 (d, 4H, *J* = 5.1 Hz), 2.45–2.57 (m, 1H), 2.63–2.72 (m, 1H), 3.09–3.14 (dd, 1H, *J* = 2.1, 2.4 Hz), 3.25–3.31 (m, 1H), 3.27–3.30 (d, 1H, *J* = 10.8 Hz), 3.85–3.88 (d, 1H, *J* = 10.8 Hz), 4.10–4.16 (dd, 1H, *J* = 6.6 Hz), 4.40–4.48 (m, 1H), 5.19 (s, 1H), 5.91 (d, 2H, *J* = 8.6 Hz), 6.81–6.84 (d, 2H, *J* = 9.0 Hz), 7.05–7.10 (t, 1H, *J* = 7.5 Hz, 7.2 Hz), 7.17–7.22 (t, 2H, *J* = 7.5 Hz), 7.31–7.33 (d, 2H, *J* = 7.2 Hz), 7.71–7.80 (m, 2H), 7.92–7.95 (d, 1H, *J* = 6.9 Hz), 8.00–8.02 (d, 1H, *J* = 8.1 Hz), 88.08–8.10 (d, 1H, *J* = 6.9 Hz), 8.17–8.20 (d, 1H, *J* = 8.1 Hz). ^{13}C NMR ($CDCl_3$, 75 MHz): δ 25.70, 28.65, 31.31, 32.79, 37.47, 40.59, 4 9.09, 52.47, 54.02, 67.40, 76.31, 113.62, 113.67, 120.87, 121.54, 123.54, 124.95 ,125.10, 126.75, 127.02, 127.35, 129.61, 130.52, 131.03, 132.04, 135.11,

141.73, 144.89, 148.42, 148.74, 167.43, 194.72, 203.91. Mass: *m*/*z* 748 (M^+). Anal. calculated for $C_{47}H_{44}N_2O_5S$: C, 75.37%; H, 5.92%; N, 3.74%; Found: C, 75.45%; H, 6.02%; N, 3.86%.

2.2.6 Spiro[2.3′]-acenapthene-1′-one-3-[4″-(3,3,6,6-tetramethyl-9-(4-nitrophenyl)-3,4,6,7,9,10-hexahydro-1,8 (2*H*,5*H*)acridinedione-10-yl)phenyl] carboxylate thiopyrrolizidine (12b)

Yield: 83%. Yellow solid, mp 210–212°C; ^{1}H NMR ($CDCl_3$, 300 MHz): δ 0.78 (s, 6H), 0.91 (s, 6H), 1.53–1.59 (d, 2H, J = 17.2 Hz), 1.81–1.87 (d, 2H, J = 17.8 Hz), 2.13–2.17 (d, 4H, J = 6.2 Hz), 2.48–2.63 (m, 1H), 2.72–2.76 (m, 1H), 3.89–3.91 (d, 1H, J = 10.6 Hz), 3.28–3.39 (m, 2H), 3.89–3.91 (d, 1H, J = 10.6 Hz), 4.17–4.18 (dd, 1H, J = 6.8 Hz), 4.42–4.56 (m, 1H), 5.25 (s, 1H), 5.96–6.0 (d, 2H, J = 8.6 Hz), 6.85–6.87 (d, 2H, J = 9.2 Hz), 7.11–7.15 (t, 1H, J = 7.5 Hz), 7.22–7.27 (t, 2H, J = 7.8 Hz), 7.36–7.38 (d, 2H, J = 7.2 Hz), 7.7–7.85 (m, 2H), 7.97–8.01 (d, 1H, J = 7.2 Hz), 8.05–8.07 (d, 1H, J = 8.4 Hz), 8.13–8.15 (d, 1H, J = 7.2 Hz), 8.22–8.25 (d, 1H, J = 8.4 Hz). ^{13}C NMR ($CDCl_3$, 75 MHz): δ 25.72, 28.68, 31.35, 31.52, 32.83, 37.51, 40.62, 49.11, 52.49, 54.08, 67.43, 76.36, 113.65, 113.69, 120.90, 121.56, 123.58, 125.01, 125.20, 127.0, 127.38, 129.81, 130.57, 131.08, 132.07, 135.17, 141.78, 144.93, 148.45, 148.79, 167.48, 194.76, 203.97. Mass: *m*/*z* 793 (M^+). Anal. calculated for $C_{47}H_{43}N_3O_7S$: C, 71.10%; H, 5.46%; N, 5.29%; Found: C, 71.21%; H, 5.54%; N, 5.37%.

2.2.7 Spiro[2.2′]-acenapthene-1′-one-3-[4′-(3,3,6,6-tetramethyl-9-phenyl-3,4,6,7,9,10-hexahydro-1,8 (2*H*,5*H*)acridinedione-10-yl)phenyl]carboxylate indolizidine (13a)

Yield: 85%. Yellow solid, mp 210–212°C; ^{1}H NMR ($CDCl_3$, 300 MHz): δ 0.75 (s, 6H), 0.90 (s, 6H), 0.83–0.86 (m, 2H), 0.95–0.98 (m, 2H), 1.28–1.33 (m, 2H), 1.71–2.28 (m 6H), 2.10–2.12 (d, 4H, J = 5.7 Hz), 2.31–2.43 (m, 2H), 3.35–3.41 (m, 1H), 3.74–3.80 (dd, 14H, J = 7.8 Hz), 5.21 (s, 1H), 6.15 (m, 2H), 6.89–6.92 (d, 2H, J = 9.0 Hz), 7.08–7.11 (d, 1H, J = 7.5 Hz), 7.19–7.24 (t, 2H, J = 7.5 Hz), 7.33–7.36 (d, 2H, J = 7.2 Hz), 7.58–7.61 (d, 1H, J = 6.9 Hz), 7.68–7.80 (m, 3H), 7.92–7.98 (m, 2H), 8.14–8.17 (d, 1H, J = 8.1 Hz). ^{13}C NMR ($CDCl_3$, 75 MHz): δ 23.74, 25.71, 26.78, 29.66, 31.90, 32.40, 32.60, 34.23, 41.74, 45.48, 46.00, 50.15, 51.04, 59.51, 72.40, 109.74, 114.73, 122.85, 123.17, 124.36, 125.91, 126.00, 127.13, 127.82, 128.08, 129.34, 129.48, 130.39, 136.32, 142.10, 145.95, 149.73, 150.46, 170.15, 180.26, 195.98. Mass: *m*/*z* 744 (M^+). Anal. calculated for $C_{49}H_{48}N_2O_5$: C, 79.01%; H, 6.49%; N, 3.76%; Found: C, 79.12%; H, 6.60%; N, 3.88%.

2.2.8 Spiro[2.2′]-acenapthene-1′-one-3-[4″-(3,3,6,6-tetramethyl-9-(4-nitrophenyl)-3,4,6,7,9,10-hexahydro-1,8(2*H*,5*H*)acridinedione)phenyl] carboxylate indolizidine (13b)

Yield: 86%. Yellow solid, mp 210–212°C; ^{1}H NMR ($CDCl_3$, 300 MHz): δ 0.75 (s, 6H), 0.916 (s, 6H), 0.85 (m, 2H), 0.97 (m, 2H), 1.28–1.33 (m, 2H), 1.62–1.99 (m, 4H), 1.90–1.95 (m, 2H), 2.10–2.38 (d, 4H, J = 10.5 Hz), 2.20–2.24 (m, 2H), 2.35–2.44 (m, 2H), 3.37–3.38 (m, 1H), 3.75–3.81 (dd, 1H, J = 7.8 Hz), 5.29 (s, 1H), 6.16–6.23 (d, 1H, J = 8.5 Hz), 6.94–6.91 (d, 1H, J = 8.7 Hz), 7.51–7.54 (m, 2H), 7.59–7.61 (d, 1H, J = 6.9 Hz). 7.68–7.80 (m, 3H), 7.87–7.90 (m, 1H), 7.93–7.98 (t, 2H, J = 7.5, 9.0 Hz), 8.08–8.81 (m, 2H), 8.15–8.18 (d, 1H, J = 8.4 Hz). ^{13}C NMR ($CDCl_3$, 75 MHz): δ 23.82, 25.85, 26.73, 29.58, 32.02, 32.40, 33.49, 34.57, 41.71, 45.67, 49.97, 50.95, 60.21, 77.26, 113.61, 121.39, 122.15, 122.83, 123.47, 125.00, 128.44, 128.79, 128.92, 130.12, 131.45, 131.74, 135.65, 139.30, 142.84, 146.19, 150.21, 150.242, 153.39, 170.42, 195.61, 208.12. Mass: *m*/*z* 789 (M^+). Anal. calculated for $C_{49}H_{47}N_3O_7$: C, 74.50%; H, 6.00%; N, 5.32%; Found: C, 74.62%; H, 6.11%; N, 5.41%.

2.3 Computational details

The input structures are drawn using Gaussview-5.0. [28] All the DFT computational calculations are performed using Gaussian 09 package [29]. In this work, the geometrical optimization of the molecule has been done using B3LYP/6-311g(d,p) level [26,27]. The frequency analysis is done on the optimized geometries and the results reveal that all the obtained frequencies are real which correspond to their ground state. Chem Craft software is used to portray the images of optimized geometries and the frontier molecular orbitals [30]. Using AutoDock Vina software, molecular docking analysis has been performed where DFT optimized structures have been used [31]. The three-dimensional structure of the protein is extracted from protein data bank. The PDB id for the protein is 6LU7 [32]. During docking process, a grid box with the sizes 60, 60, and 60 along the *X*-, *Y*-, and *Z*-axes is used as reported earlier [33,34]. The flow chart of the cycloaddition process has been described in

3 Results and discussion

3.1 Chemistry

The highly functionalized dipolarophiles, *O*-acryloylacridinediones **5a–b** were derived from dimedone **1** in three

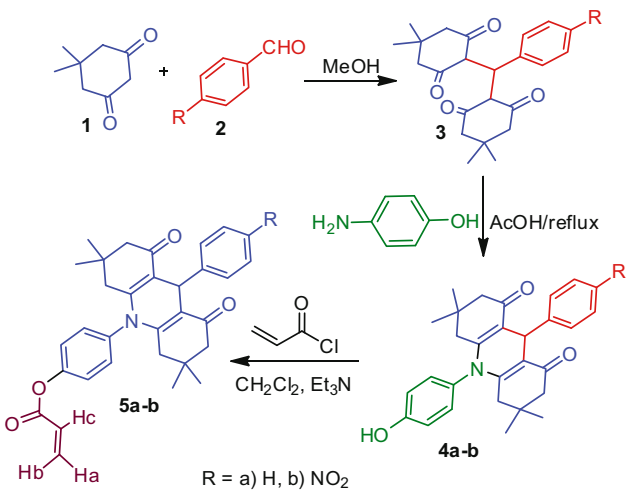

Scheme 1: Synthesis of *O*-acryloylacridinedione dipolarophiles, **5a–b**.

good yielding steps [35] as shown in Scheme 1. Primarily, the reaction of dimedone **1** and aromatic aldehyde **2** in methanol afforded 4-hydroxyphenyl tetraketone **3** which was cyclized with 4-aminophenol in acetic acid to give the acridinediones **4a–b**. The *O*-acylation of **4** with acryloyl chloride in CH_2Cl_2 in the presence of Et_3N at 0°C to room temperature afforded *O*-acryloyl acridinediones **5a–b** in good yields. The structure of the compounds was fully characterized by NMR spectroscopic data. In the ^{1}H NMR spectrum of compound **5a**, the two doublets at δ 6.10 and δ 6.66 were assigned to H_a and H_b of allyl $-CH_2$ protons and a doublet of doublets at δ 6.33 to H_c proton. The ^{13}C NMR spectrum of compound **5a** showed a signal at δ 133.6 ppm due to the allyl $-CH_2$, while the ester carbonyl group resonated at δ 163.95 ppm. The *gem*-dimethyl carbons resonated

Table 1: Solvent optimization of mono-spirocycloadduct, **8a**

Entry	Solvents	Time (h)	Yield (%)
1	Methanol	12	47
2	1,4-Dioxane	18	12
3	Acetonitrile	8	89
4	Toluene	16	—
5	THF	12	34
6	[Bmim]Br	5	92

at δ 26.77 and δ 29.74 ppm and two methylene carbons appeared at δ 41.82 and δ 50.21 ppm.

With the acridinedione dipolarophiles in hand, to start with the three-component cycloaddition reaction, initially in order to optimize the reaction conditions, a representative reaction was carried out involving isatin **6**, thiazolidine-4-carboxylc acid **7**, and *O*-acryloyl acridinedione **5a** with various solvent system such as methanol, 1,4-dioxane, acetonitrile, toluene, and tetrahydrofuran (Table 1). The reaction of isatin **6**, thiazolidine-4-carboxylc acid **7** via a decarboxylative pathway furnished the 1,3-dipole component which in turn added regioselectivity to **5a**. Thus, a mixture of **5a**, **6**, and **7** in 5 mL of CH_3CN was refluxed for 8 h. After all starting materials had completely disappeared as indicated by TLC analysis, the crude product was purified by column chromatography and it was observed that among these solvents, the reaction in CH_3CN gave the best yield of the product **8a** (89%) than the other solvents. Since the main goal of organic synthesis is to develop a new synthetic strategy using green solvents, we performed the same reaction in an ionic liquid, [Bmim]Br and expected, a quantitative yield of **8a** (92%) in [Bmim]Br was observed in a significantly shorter reaction time (5 h) (Scheme 2, Table 1).

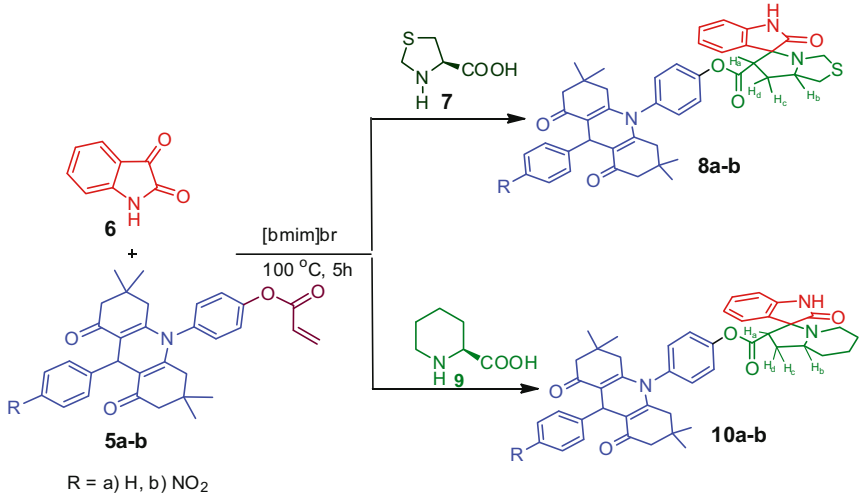

Scheme 2: Synthesis of spirooxindolothiopyrrolizidines/indolizidines, **8–10**.

Subsequently, all other reactions were executed with the ionic liquid. It is pertinent to note that ionic liquids are eco-friendly green solvents because of their lower vapor pressure, good solvating capacity, high thermal and chemical stability, good solvating ability, non-coordinating nature, and easy recyclability which make them a good choice for various chemical reactions. In addition, ionic liquids have attracted tremendous attention in recent years due to their identification and tunable properties as green solvents, catalysts, and reagents. It is important to note that ionic liquids act as both catalysts and solvents in various synthetic transformations.

The structure and the regiochemistry of the cycloadducts were unambiguously established by their spectroscopic analysis. The ^{1}H NMR spectrum of compound **8a** showed a multiplet in the range δ 4.34–4.38 for H_b proton. The H_a proton was observed as a doublet of doublets at δ 3.97–4.03 (J = 6.6, 6.9 Hz). If another isomer was formed, one would expect a multiplet instead of a doublet of doublet. The H_c and H_d protons appeared as a multiplet in the range δ 2.32–2.44 and δ 2.54–2.62, respectively. The methylene proton flanked between the nitrogen and sulfur atom appeared as two doublets at δ 3.48 and 3.90. The –NH proton of the oxindole ring resonated at δ 9.05 ppm as a singlet. The *gem*-dimethyl proton showed two singlets at δ 0.77 and 0.92 ppm for acridinedione moiety. The ^{13}C NMR spectrum of **8a** exhibited a peak at δ 180.44 ppm due to acridinedione carbonyl carbon. The two peaks at δ 168.44 and 196.08 ppm were due to oxindole and ester carbonyl carbons. A peak at δ 73.97 ppm was accounted for the spiro carbon of oxindole moiety. The DEPT 135 spectrum showed peaks at δ 33.46, 38.17, 41.72, 50.13, and 55.00 ppm in negative region for the five methylene carbons present in the cycloadducts (Figure 2).

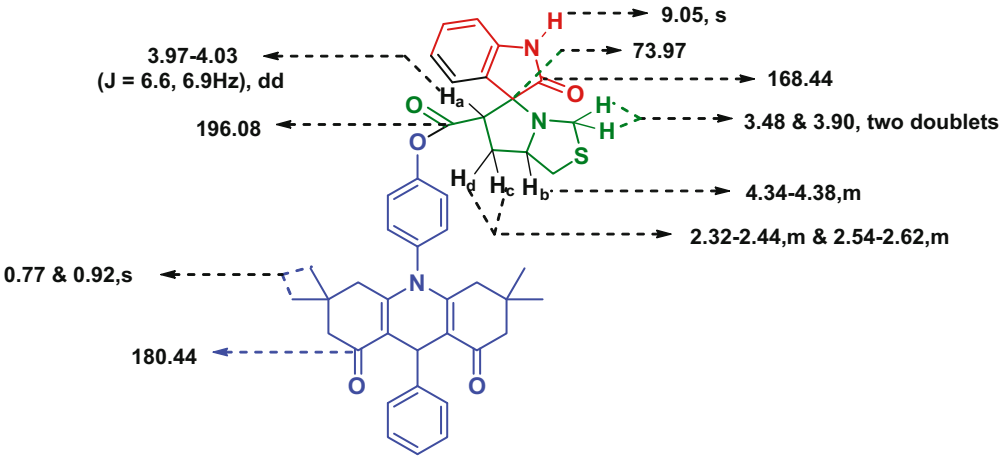

Figure 2: Selected ^{1}H and ^{13}C NMR chemical shifts of **8a**.

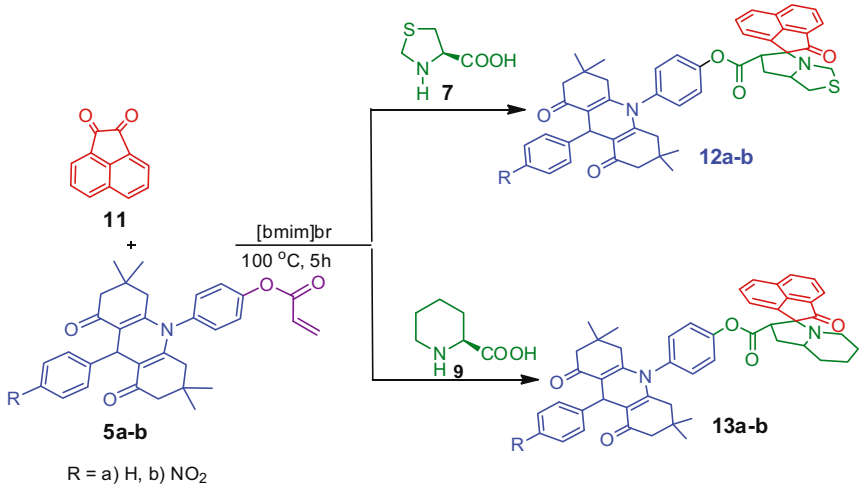

Scheme 3: Synthesis of acenaphthenopyrrolizidines/indolizidines, **12–13**.

Table 2: Cycloaddition of ylides generated from di ketones and secondary amino acids with the dipolarophiles, **5a–b**

Entry	Dipolarophile	Diketone	*Sec*-amino acid	Products	Time (h)	Yield (%)[a]
1	**5a**	6	7	**8a**	5	84
2	**5b**	6	7	**8b**	4.5	87
3	**5a**	6	9	**10a**	4	79
4	**5b**	6	9	**10b**	3.5	81
5	**5a**	11	7	**12a**	4	80
6	**5b**	11	7	**12b**	3.5	83
7	**5a**	11	9	**13a**	5	85
8	**5b**	11	9	**13b**	4.5	86

[a]Isolated product after column chromatography.

We extended the same methodology for the synthesis of a novel mono spirooxindoloindolizidines **10a–b**. The non-stabilized azomethine ylide generated *in situ* from isatin **6** with pipecolinic acid **9**, underwent cycloaddition with *O*-acryloyl acridinedione **5a–b** in ionic liquids, [Bmim]Br condition to afford mono spirooxindoloindolizidines **10a–b** in good yields (Scheme 2). No trace of the other possible regioisomer was observed even after prolonged reaction time. The structure and regiochemistry of the products **10a–b** were established by IR, ^{1}H and ^{13}C NMR spectroscopy analysis. The ^{1}H NMR spectrum of compound **10b** exhibited a multiplet in the range of δ 3.23–3.29 for H_b proton. The doublet of doublet appeared at δ 3.70 due to H_a proton confirmed the regio chemistry of the cycloaddition. The H_c and H_d protons resonated at δ 2.30–2.53 as a multiplet. The –NH proton of the oxindole ring resonated at δ 7.78 as a singlet. The *gem*-dimethyl proton showed two singlets at δ 0.77 and 0.94 for acridinedione moiety. In the ^{13}C NMR spectrum of cycloadduct **10b**, the ester and oxindole carbonyl carbon were resonated at 195.84 and 170.10 ppm, respectively. The acridinedione carbonyl carbon appeared at 180.26 ppm and the spiro quaternary carbon of oxindole ring appeared at 72.40 ppm. In DEPT 135 studies confirmed the presence of seven methylene carbons in cycloadduct which appeared at 23.72, 25.69, 31.88, 34.21, 41.89, 45.48, and 49.97 ppm.

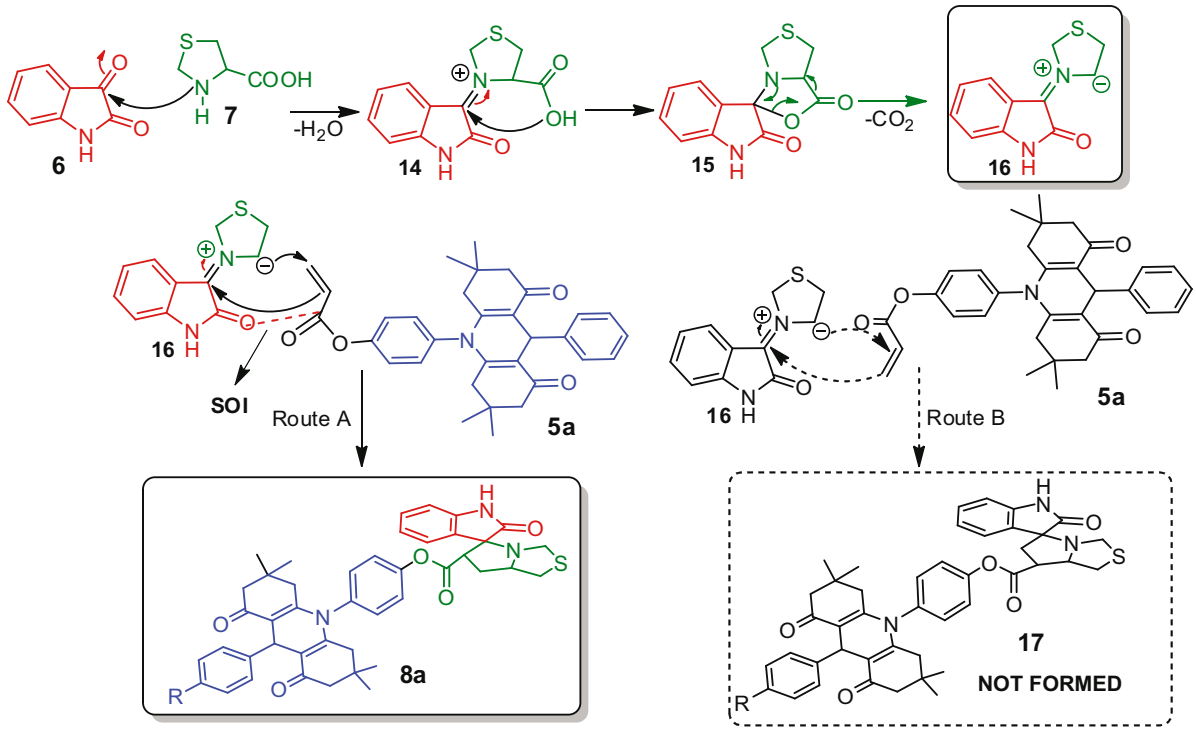

Scheme 4: Persuasive mechanism for the synthesis of spiroheterocyclic hybrids.

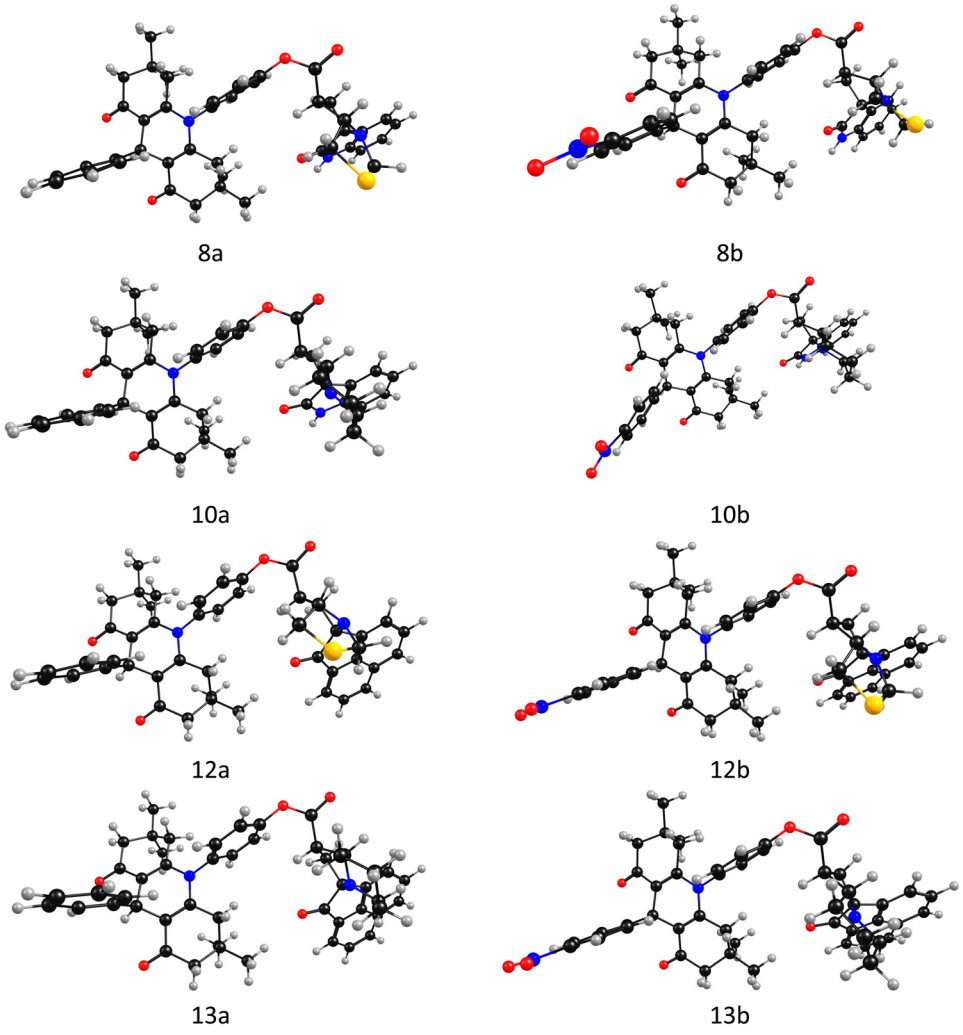

Figure 3: Optimized geometry of the molecules.

The utility of acridinedione dipolarophiles **5a–b** in the preparation of diverse spiroheterocyclic hybrids were further explored by executing the cycloaddition process with different diketone, acenaphthenequinone **11**. Thus, an equimolar mixture of acenapthequinone **11**, thiazolidine-4-carboxylc acid **7**/pipecolinic acid **9**, and *O*-acryloylacridinedione **5a–b** refluxed in [Bmim]Br at 100°C resulted in the formation of spiroacenapthenothiopyrrolizidines **12a–b**/indolizidines **13a–b** in good yield (Scheme 3, Table 2). The formation of the products was confirmed by the spectroscopic analysis.

A plausible reaction pathway for the formation of the spirohybrid heterocycles **8–10** and **12–13** is described in Scheme 4 considering a representative case **8a**. Initially, the condensation reaction of isatin **6** and thiazolidine-4-carboxylic acid **7** afforded the iminium ion intermediate **14** by dehydration. The spirooxazolidinone **15** derived from **14** afforded the reactive azomethine ylide **16** by decarboxylation. The cycloaddition reaction of the 1,3-dipole component **16** and the alkene **5a**, may occur either via route A or route B. However, the exclusive formation of spirooxindolothiopyrrolizidines **8a** revealed that route A is favored than route B. In route A, the amide carbonyl group of the 1,3-dipole **16** having secondary orbital interaction (SOI) [36] with the carbonyl group of dipolarophile **5a** with ylide **16**, whereas in route B such kind of SOI was ruled out because the carbonyl group of dipole **16** is far away from the carbonyl group of dipolarophile **5a**. In addition, the regioselectivity product **8a** was observed and other possible regioisomer **17** was not formed since the electron rich dipole **16** preferentially attacks the electron deficient β-carbon of **5a** affording **8a**. The resulting cycloadduct obtained possesses three sterogenic carbons that have a spiro carbon via the generation of one C–N and two C–C in a one-pot reaction sequence.

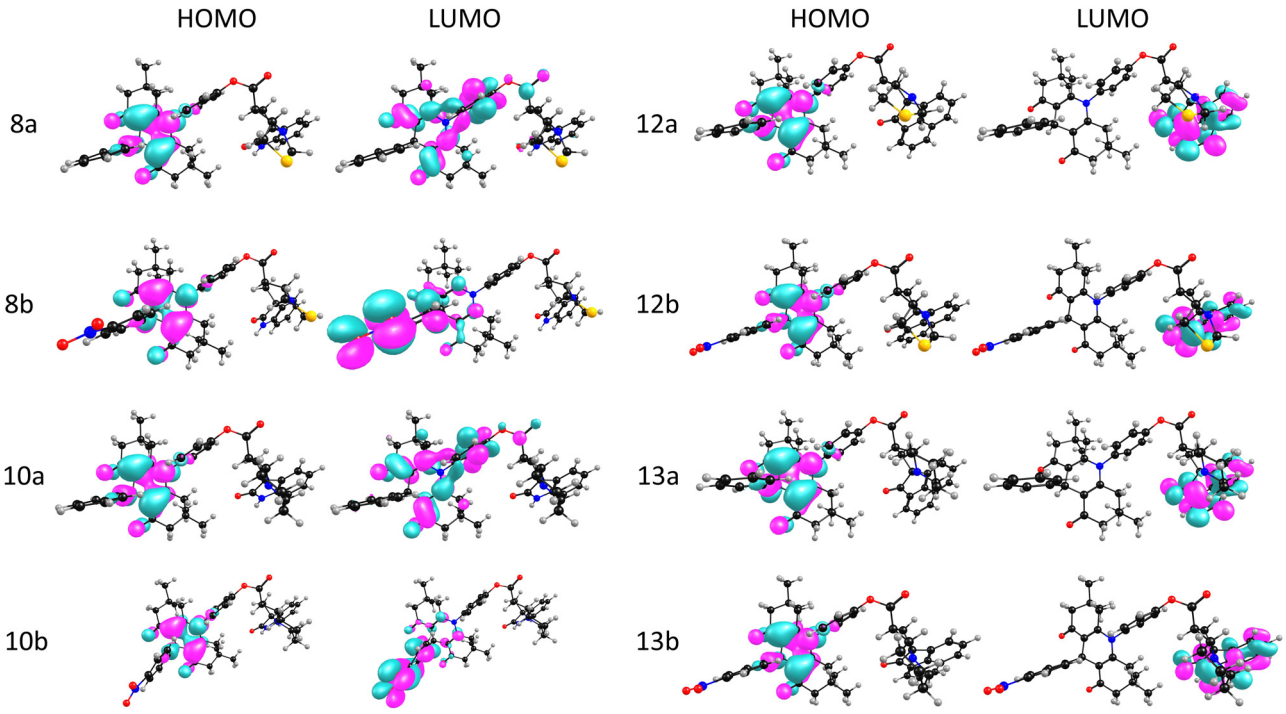

Figure 4: Frontier molecular orbitals of the molecules.

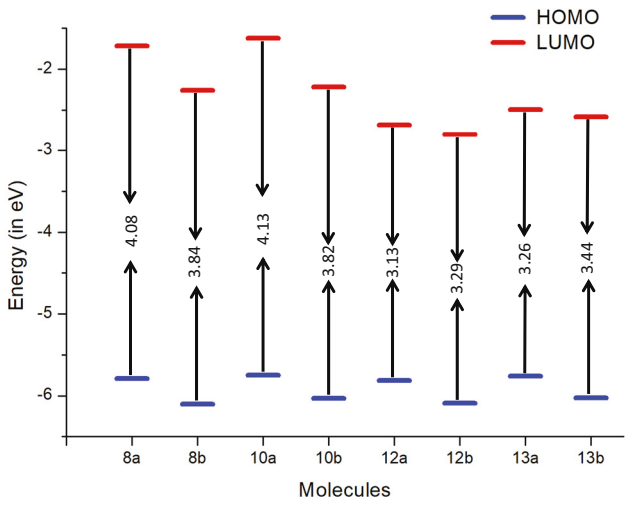

Figure 5: HOMO–LUMO energy gap of the molecules.

3.2 Geometrical analysis

The optimized geometry of the molecules is given in Figure 3. From the figure, it is clear that the molecules are not planar and are twisted. The molecules are twisted due to the presence of C–C single bonds between moieties. All the molecules are twisted by an angle of ~154°. The bond length of C═O in all the molecules is observed to be at around 1.91 Å. In all the molecules, the oxygen flanked between the carboxyl group and the benzene is acting as a conjugation stopper. In molecules **8a**, **8b**, **10a**, and **10b**, the hydrogen of –NH group can be easily abstracted. For instance, in these molecules the –NH bonds are having a length of 1.01 Å while the usual –NH bond is 1.00 Å. Thus, due to this –NH elongation in these molecules the hydrogen atoms can be abstracted.

3.2.1 Frontier molecular orbitals analysis

Highest occupied molecular orbital (HOMO) and lowest unoccupied molecular orbital (LUMO) of the molecules are given in Figure 4. It can be seen that the HOMO of the molecules is localized on the hexahydro acridine dione moiety. The LUMO of 8a and 10a is localized on the hexahydro acridine dione and the benzoic acid moieties, whereas on substitution of NO_2 in the 8b and 10b molecules the LUMO gets localized on phenyl and hexahydro acridine dione moieties. In the case of 12a, 12b, 13a, and 13b molecules the LUMO is localized on acenaphthylenone moiety. The HOMO–LUMO energy gap is depicted in Figure 5. The HOMO–LUMO gap is greatest in 10a (4.13 eV) and lowest in 12b (3.13 eV). Thus, 10a molecule is the most stable and 12b molecule is expected to be highly active with a low HOMO–LUMO gap among all the molecules. The HOMO–LUMO gap values are in the range of 3.13–4.13 eV.

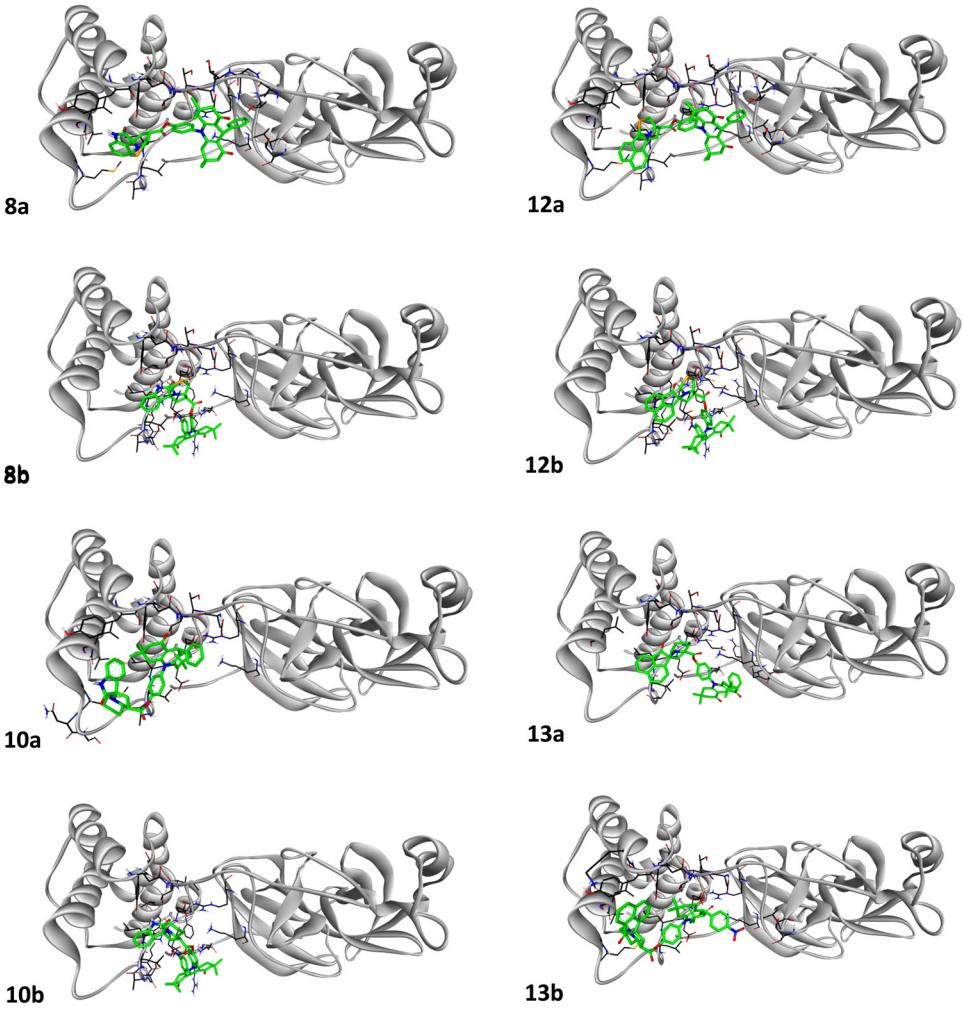

Figure 6: Molecular docking studies on the best possible binding position of molecules in the protein.

3.2.2 Molecular docking

Drug designing industry largely depends on computer-aided tools in predicting the activity of drugs at molecular level. One such important tool is molecular docking analysis which is used to find out the binding modes of the drugs, inhibitors, ligands, and metal complexes toward the protein [37]. Therefore, molecular docking analysis in combination with density functional theory calculations is carried out. Results of molecular docking reveal that the 8b molecule shows better binding ability than the other molecules. 8b has the highest binding energy with −10.4 kcal·mol^{-1}. The most favorable docking pose of ligand–protein for all molecules is given in Figure 6. The decreasing order of binding energies in the synthesized molecules is 8b > 12a > 12b > 10b, 13a > 8a > 10a, 13b. The representation of the interactions of the molecules with amino acids of the protein for all is given in Figure 7. The results obtained from Figures 6 and 7 are discussed below. The binding pocket of 8a consists of the following resides: Thr 199, Asn 238, Thr 196, Asp 197, Ala 194, Val 171, Thr 135, Asn 133, Thr 169, Agr131, Lys 137, Tyr 239, Leu 286, Leu 287, Met276, Gly 275, Leu 271, Leu 272, and Tyr 237. The ligand 8a has one π-donor hydrogen bond with Asn 133, two π-sigma interactions with Leu 287 and Val 171 and one π-alkyl interaction with Ala 194. In 8b Leu 286 has three interactions: π-sigma interaction and two π-alkyl interactions. Apart from this 8b has a π-donor hydrogen bond with Leu 287 and a π-alkyl interaction with Ala 285. Also, 8b has a conventional hydrogen bond with Lys 137 with a distance of 2.00 Å. For 10a conventional hydrogen bonds are observed with Arg 131 (2.80 Å) and Asn (2.09 Å), two π-alkyl interactions with Leu 286 and a π-alkyl interaction with Met 276. 10b has a conventional hydrogen bond with Trp 207 having a distance of 2.20 Å and three π-alkyl interactions with Leu 286. The molecule 12a has one conventional hydrogen bond (Tyr 239) with a distance of 2.13 Å, one π-sigma interaction (Val 171) and five π-alkyl interactions (Asp 197, Ala 194, Leu 286, Met 276, and Leu 287). 12b molecule has three interactions with Leu 286 (one

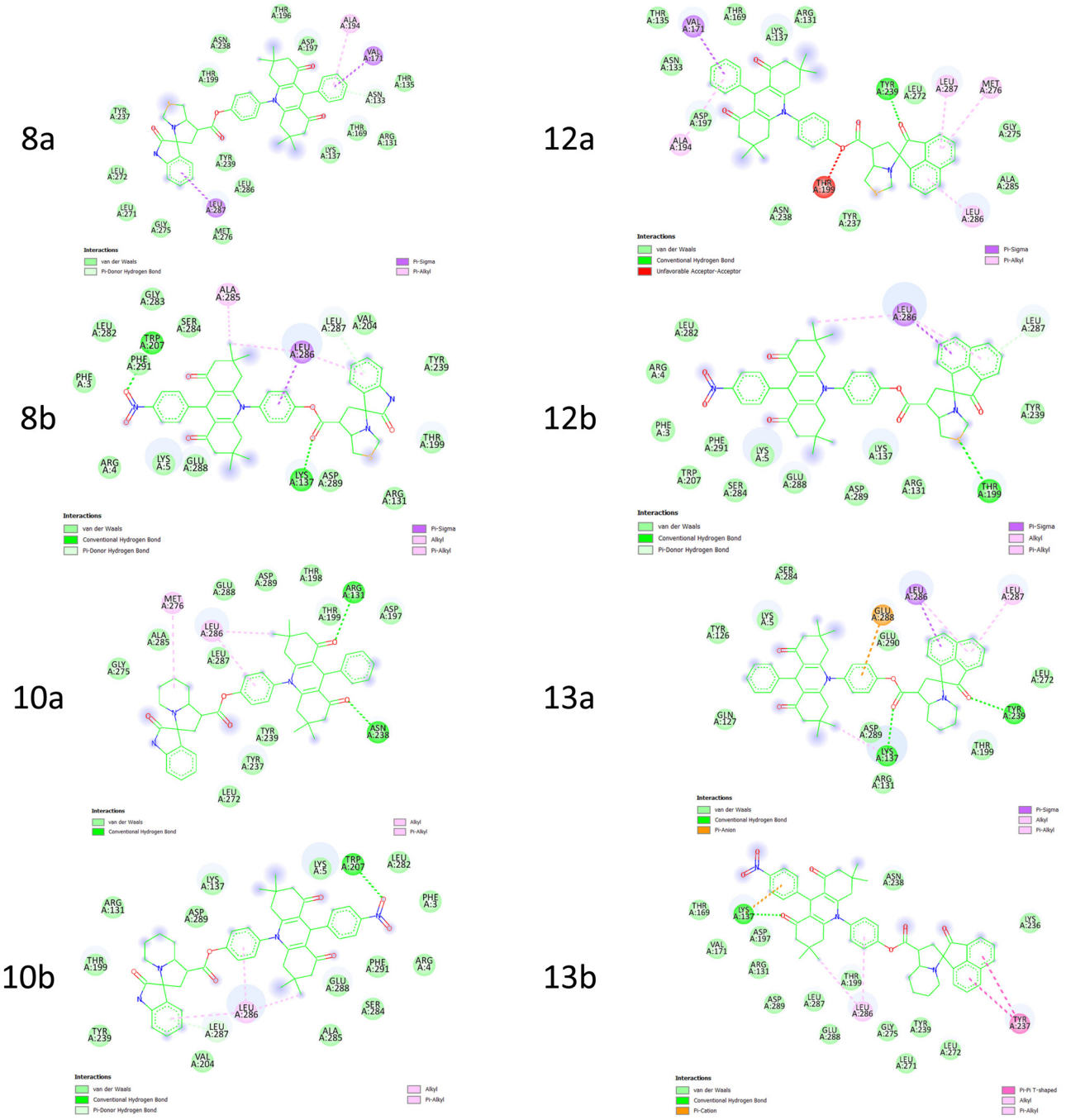

Figure 7: Schematic representation of interaction of spirocompounds with the protein.

π-sigma interaction and two π-alkyl interactions). Apart from this 12b has a conventional hydrogen bond with Thr 199 having a bond distance of 3.06 Å. For 13a molecule one π-anion interaction with Glu 288, one π-sigma interaction with Leu 286 and three π-alkyl interactions with Lys 137, Leu 286, and Leu 287 is observed. 13a also has two conventional hydrogen bonds with Lys 137 (2.66 Å) and Tyr 239 (2.62 Å). The 13b molecule has two π–π T-shaped interactions with Tyr 237, two π-alkyl interactions with Leu 286, one π-cation interaction with Lys 137 and one conventional hydrogen bond with Lys 137 (2.62 Å). Thus, all the ligands are stabilized by hydrogen bonding, π–π interactions and electrostatic interactions. Hence, all these molecules are promising inhibitors for COVID-19 drug discovery and further experimental studies have to be done in order to prove their utility.

4 Conclusion

A series of structurally intriguing new class of acridinedione embedded spirooxindolothiazolidine/indolizidine and spiroacenapthenothiazolidine/indolizidine has been synthesized in quantitative yields employing ionic liquid supported eco-friendly green protocol. The cycloaddition protocol was investigated under various solvent systems and observed that ionic liquids are better yield than other organic solvents. The cycloaddition protocol generated three stereogenic carbons, out of three one is spiro carbon via the formation of C–N and two C–C bonds in single synthetic transformation. These cycloadducts were unambiguously assigned by spectroscopic analysis. Geometrical parameters of the synthesized compounds were investigated using the B3LYP/6-311g(d,p) level of theory. Molecular simulation was performed to understand the binding affinity of spiro compounds with protein. The molecules are stabilized by hydrogen bonding interactions along with other non-covalent interactions and results reveal that spiro compound **8b** binds to the protein more readily than the other compounds. As spiroheterocycles are prime compounds with unique structural features, the current methodology described in this study can be adopted for the synthesis of similar spiroheterocycles with diverse substitutions and can be evaluated multifarious biological assays.

Funding information: The project was funded by Researchers Supporting Project Number (RSP2023R143), King Saud University, Riyadh, Saudi Arabia.

Author contributions: Rajesh Raju, Raghavachary Raghunathan, and Natarajan Arumugam: conceptualization, investigation, supervision, formal analysis, methodology, validation, writing – original draft, visualization; Raju Suresh Kumar: methodology, validation, writing – review and editing; Abdulrahman I. Almansour: project administration, visualization, writing – review and editing; P.A. Vivekanand: writing – review and editing; Cheriyan Ebenezer and Rajadurai Vijay Solomon: validation, writing – review and editing. Karthikeyan Perumal: investigation, formal analysis, methodology.

Conflict of interest: The authors state no conflict of interest.

Data availability statement: All materials for this study are presented in this article and available on request to the corresponding author.

References

[1] Rotella DP. Chapter four – heterocycles in drug discovery: properties and preparation. Adv Hetrocycl Chem. 2021;134:149–83.
[2] Zheng YJ, Colin MT. The utilization of spirocyclic scaffolds in novel drug discovery. Expert Opin Drug Discov. 2016;11:831–4. doi: 10.1080/17460441.2016.1195367.
[3] Almansour AI, Arumguam N, Suresh Kumar R, Al-thamili DM, Periyasami G, Ponmurugan K, et al. Domino multicomponent approach for the synthesis of functionalized spiro-indeno[1,2-b] quinoxaline heterocyclic hybrids and their antimicrobial activity, synergistic effect and molecular docking simulation. Molecules. 2019;24:1962. doi: 10.3390/molecules24101962.
[4] Suresh Kumar R, Almansour AI, Arumugam N, Kotresha D, Manohar TS, Venketesh S. Cholinesterase inhibitory activity of highly functionalized fluorinated spiropyrrolidine heterocyclic hybrids. Saudi J Biol Sci. 2021;28:754–61.
[5] Suresh Kumar R, Almansour AI, Arumugam N, Mohammad F, Ranjith Kumar R. In vitro mechanistic exploration of novel spiropyrrolidine heterocyclic hybrids as anticancer agents. Front Chem. 2020;8:465.
[6] Arumugam N, Almansour AI, Suresh Kumar R, Alaqeel SI, Krishna VS, Sriram D. anti-tubercular activity of novel class of spiropyrrolidine tethered indenoquinoxaline heterocyclic hybrids. Bioorg Chem. 2020;99:103799. doi: 10.1016/j.bioorg.2020.103799.
[7] Lawson S, Arumugam N, Almansour AI, Suresh Kumar R, Thangamani S. Dispiropyrrolidine tethered piperidone heterocyclic hybrids with broad-spectrum antifungal activity against *Candida albicans* and *Cryptococcus neoformans*. Bioorg Chem. 2020;100:103865. doi: 10.1016/j.bioorg.2020.103865.
[8] Bolous M, Arumugam N, Almansour AI, Suresh Kumar R, Maruoka R, Antharam VC, et al. Broad-spectrum antifungal activity of spirooxindolo-pyrrolidine tethered indole/imidazole hybrid heterocycles against fungal pathogens. Bioorg Med Chem Lett. 2019;29:2059–63. doi: 10.1016/j.bmcl.2019.07.022.
[9] Arumugam N, Almansour AI, Suresh Kumar R, Periasamy VS, Athinarayanan J, Alshatwi AA, et al. Regio- and diastereoselective synthesis of anticancer spirooxindoles derived from tryptophan and histidine via three-component 1,3-dipolar cycloadditions in an ionic liquid. Tetrahedron. 2018;74:5358–66. doi: 10.1016/j.tet.2018.04.032.
[10] Shahidul Islam M, Al-Majid AM, El-Senduny FF, Badria FA, Motiur Rahman AFM, Barakat A, et al. Synthesis, anticancer activity, and molecular modeling of new halogenated spiro[pyrrolidine-thiazolo-oxindoles] derivatives. Appl Sci. 2020;10(6):2170. doi: 10.3390/app10062170.
[11] Michael JP. Indolizidine and quinolizidine alkaloids. Nat Prod Rep. 2001;18:520–42. doi: 10.1039/B005384H.
[12] Pulici M, Quartieri F. Traceless solid-phase synthesis of 2-amino-5-alkylidene-thiazol-4-ones. Tetrahedron Lett. 2005;46:2387–91. doi: 10.1016/j.tetlet.2005.02.059.
[13] Bonde CG, Gaikwad NJ. Synthesis and preliminary evaluation of some pyrazine containing thiazolines and thiazolidinones as antimicrobial agent. Bioorg Med Chem. 2004;12:2151–61. doi: 10.1016/j.bmc.2004.02.024.
[14] Kucukguzel SG, Oruc EG, Rollas S, Sahin F, Ozbek A. Synthesis, characterization and biological activity of novel 4-thiazolidinones,

1,3,4-oxadiazoles and some related compounds. Eur J Med Chem. 2002;37:197–206. doi: 10.1016/S0223-5234(01)01326-5F:\EDITING \gps-2023-0036\10.1016\S0223-5234 (01)01326-5.

[15] Rajesh R, Raghunathan R. Expeditious synthesis of novel β-lactam-substituted polycyclic fused chromenopyrrole derivatives from MBH carbonates by intramolecular [3 + 2]-cycloaddition reaction. Synlett. 2013;24:2107–13. doi: 10.1055/s-0033-1339519.

[16] Rajesh R, Raghunathan R. Synthesis of β-lactam tethered polycyclic fused heterocycles through a rearrangement by a one pot tandem [3 + 2]-cycloaddition reaction. Eur J Org Chem. 2013;2597–607. doi: 10.1002/ejoc.201201471.

[17] Arumugam N, Almansour AI, Suresh Kumar R, Alaqeel SI, Siva Krishna V, Sriram D. Anti-tubercular activity of novel class of spiropyrrolidine tethered indenoquinoxaline heterocyclic hybrids. Bioorg Chem. 2020;99:103799. doi: 10.1016/j.bioorg.2020.103799.

[18] Arumugam N, Almansour AI, Suresh Kumar R, Mohammad Ali Al-Aizari AJ, Alaqeel SI, Kansız S, et al. Regio-and diastereoselective synthesis of spiropyrroloquinoxaline grafted indole heterocyclic hybrids and evaluation of their anti-*Mycobacterium tuberculosis* activity. RSC Adv. 2020;10:23522–31. doi: 10.1039/D0RA02525A.

[19] Arumugam N, Almansour AI, Suresh Kumar R, Kotresha D, Saiswaroop R, Venketesh S. Dispiropyrrolidinyl-piperidone embedded indeno[1,2-b]quinoxalineheterocyclic hybrids: synthesis, cholinesterase inhibitory activity and their molecular docking simulation. Bioorg Med Chem. 2019;27:2621–8. doi: 10.1016/j.bmc.2019.03.058.

[20] Sumesh RV, Muthu M, Arumugam N, Almansour AI, Suresh Kumar R, Athimoolam S, et al. Multicomponent dipolar cycloaddition strategy: combinatorial synthesis of novel spiro-tethered pyrazolo[3,4-b]quinolinehybrid heterocycles. ACS Comb Sci. 2016;18:262–70. doi: 10.1021/acscombsci.6b00003.

[21] Rajesh R, Suresh M, Selvam R, Raghunathan R. Synthesis of acridinedione derived mono spiro-pyrrolidine/pyrrolizidine derivatives-a facile approach via intermolecular [3 + 2]-cycloaddition reaction. Tetrahedron Lett. 2014;55:4047–53. doi: 10.1016/j.tetlet.2014.05.133.

[22] Girault S, Grellier P, Berecibar A, Maes L, Mouray E, Lemiere P, et al. Antimalarial, anti-trypanosomal, and antileishmanial activities and cytotoxicity of bis(9-amino-6-chloro-2-methoxyacridines): influence of the linker. J Med Chem. 2000;43:2646–54. doi: 10.1021/jm990946n.

[23] Sánchez I, Reches R, Henry D, Pierre C, Maria R, Pujol D. Synthesis and biological evaluation of modified acridines: the effect of N- and O-substituent in the nitrogenated ring on antitumor activity. Eur J Med Chem. 2006;41:340–52. doi: 10.1016/j.ejmech.2005.11.006.

[24] Yang P, Yang Q, Qian X, Tong L, Li X. Isoquino[4,5-bc]acridines: design, synthesis and evaluation of DNA binding, anti-tumor and DNA photo-damaging ability. J Photochem Photobiol. 2006;B84:221–6. doi: 10.1016/j.jphotobiol.2006.03.005.

[25] Gallermann G, Rudi A, Kashman Y. Synthesis of pyrido[2,3,4-kl] acridines a building block for the synthesis of pyridoacridine alkaloids. Tetrahedron Lett. 1992;33:5577. doi: 10.1016/S0040-4039(00)61150-4.

[26] Clementi E, André JM, McCammon JA. Theory and applications in computational chemistry: the first decade of the second millennium. Italy: American Institute of Physics; 2012.

[27] Rouhani M. Evaluation of structural properties and antioxidant capacity of Proxison: a DFT investigation. Comput Theor Chem. 2021;1195:113096.

[28] Roy D, Todd A, John M. Gauss View 5.0. 8, Wallingford: Gaussian, Inc., 2009.

[29] Frisch MJ. Gaussian09; 2009. http://www.gaussian.com/.

[30] Zhurko G. ChemCraft software, version 1.6; 2014.

[31] Trott O, Olson AJ. AutoDock Vina: improving the speed and accuracy of docking with a new scoring function, efficient optimization, and multithreading. J Comput Chem. 2010;31:455–61.

[32] Jin Z, Du X, Xu Y, Deng Y, Liu M, Zhao Y, et al. Structure of M pro from SARS-CoV-2 and discovery of its inhibitors. Nature. 2020;582:289–93.

[33] Sankarganesh M, Raja JD, Revathi N, Solomon RV, Kumar RS. Gold (III) complex from pyrimidine and morpholine analogue Schiff base ligand: sSynthesis, characterization, DFT, TDDFT, catalytic, anticancer, molecular modeling with DNA and BSA and DNA binding studies. J Mol Liq. 2019;294:111655.

[34] Nehru S, Anitha Priya JA, Hariharan S, Vijay Solomon R, Veeralakshmi S. Impacts of hydrophobicity and ionicity of phendione-based cobalt(II)/(III) complexes on binding with bovine serum albumin. J Biomol Struct Dyn. 2020;38:2057–67.

[35] Srividya N, Ramamurthy P, Shanmugasundaram P, Ramakrishnan VT. Synthesis. characterization, and electrochemistry of some acridine-1,8-dione dyes. J Org Chem. 1996;61:5083–9. doi: 10.1021/jo9600316.

[36] Rao JNS, Raghunathan R. An expedient diastereoselective synthesis of pyrrolidinyl spirooxindoles fused to sugar lactone via [3+2] cycloaddition of azomethine ylides. Tetrahedron Lett. 2012;53:854–8. doi: 10.1016/j.tetlet.2011.12.025.

[37] Ambika S, Manojkumar Y, Arunachalam S, Gowdhami B, Sundaram KKM, Solomon RV, et al. Biomolecular interaction, anticancer and anti-angiogenic properties of cobalt(III) schiff base complexes. Sci Rep. 2019;9:2721.

Appendix

A1 Selected ^{1}H and ^{13}C NMR spectra of the spirocompounds

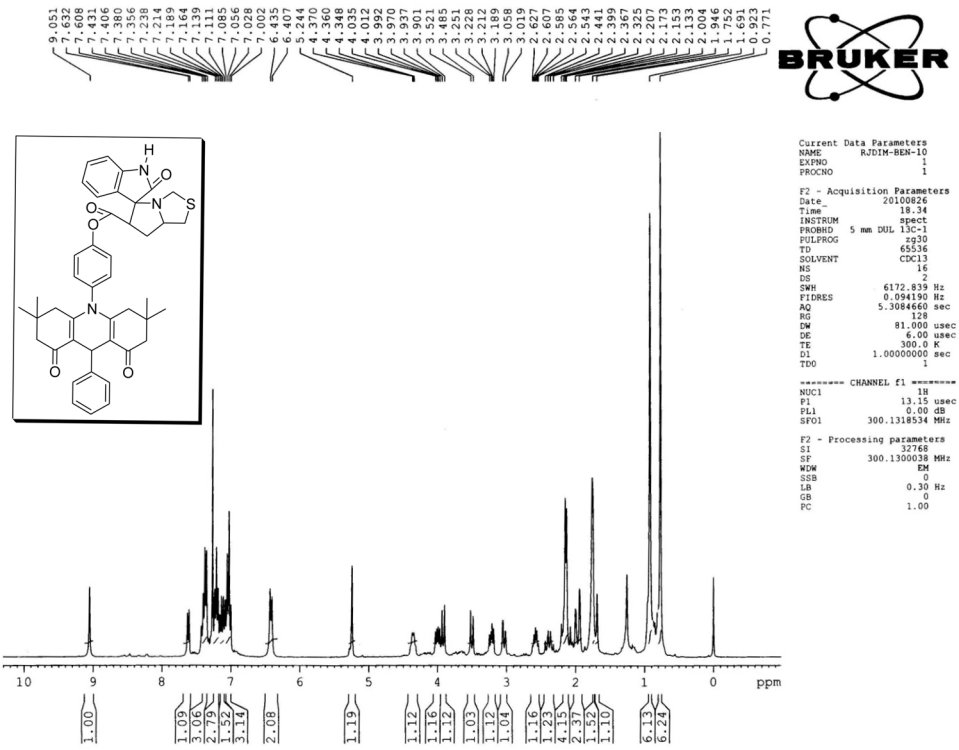

Figure A1: ^{1}H NMR spectrum of compound **8a**.

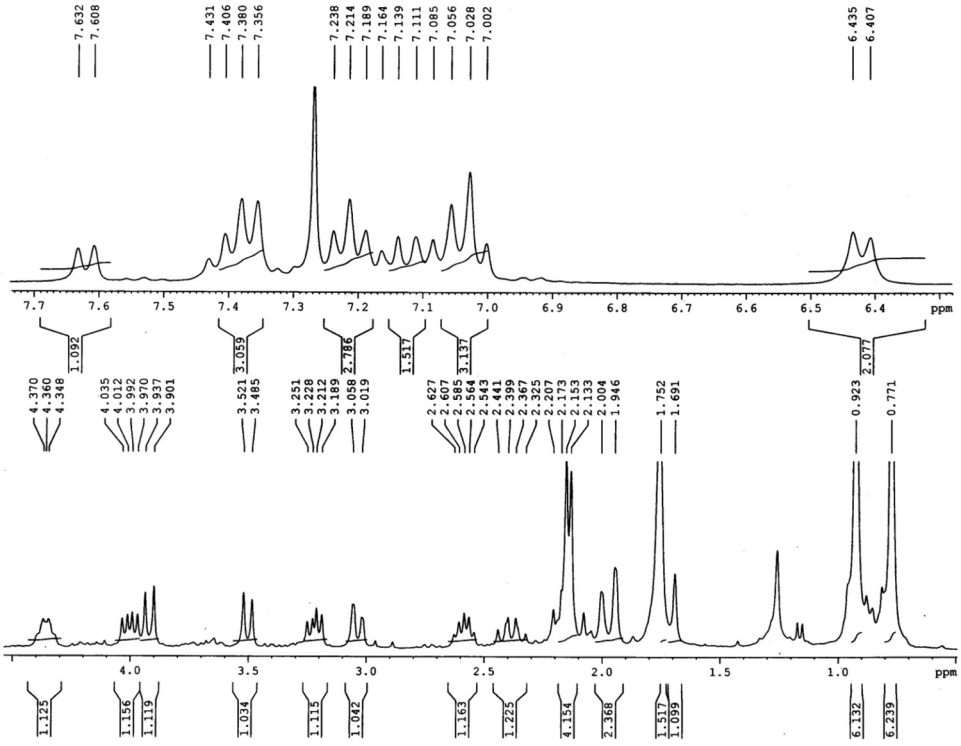

Figure A2: ^{1}H NMR expansion spectrum of compound **8a**.

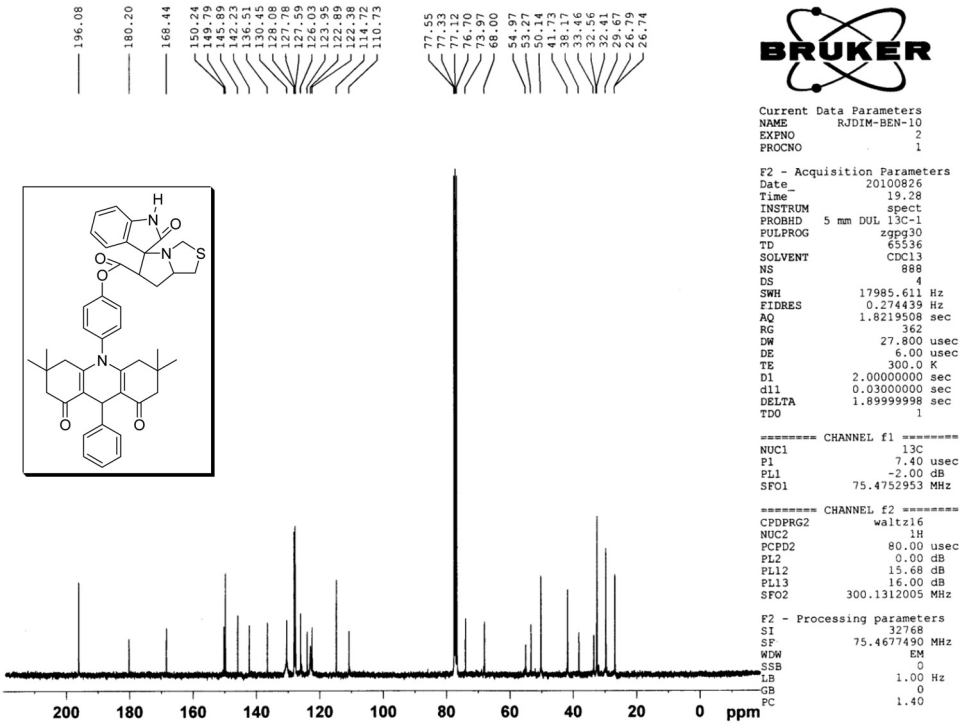

Figure A3: ^{13}C NMR spectrum of compound **8a**.

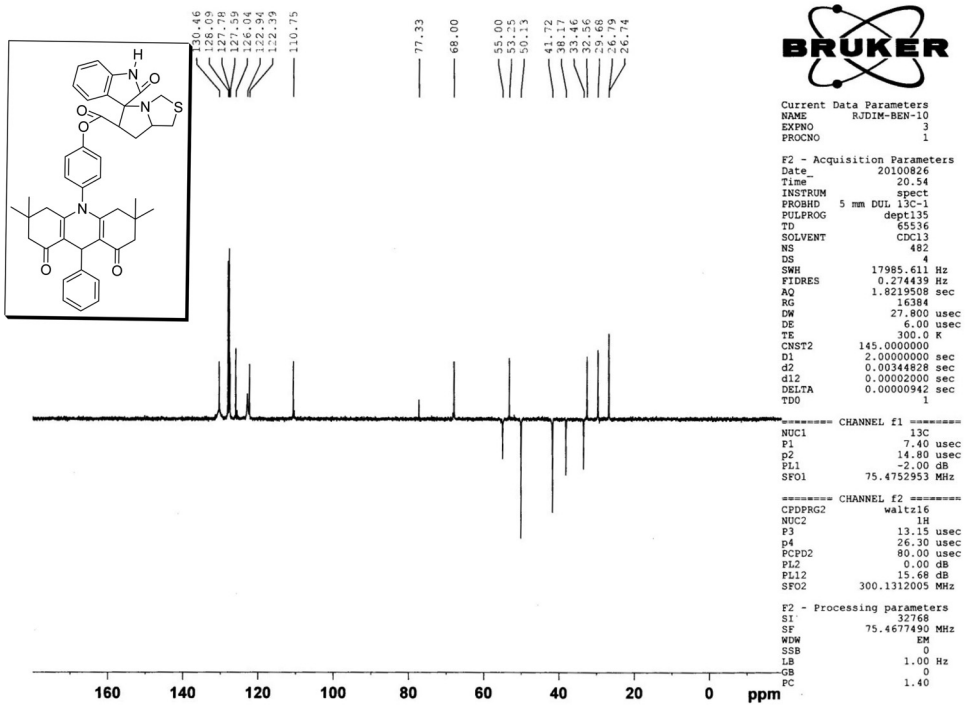

Figure A4: DEPT 135 NMR spectrum of compound **8a**.

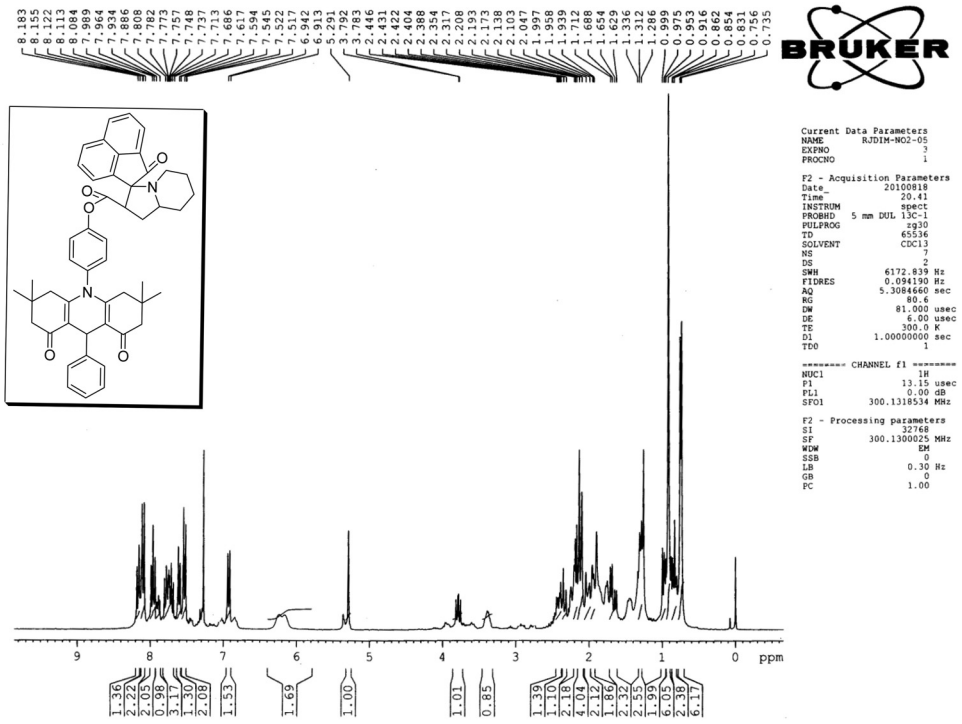

Figure A5: [1]H NMR spectrum of compound **13a**.

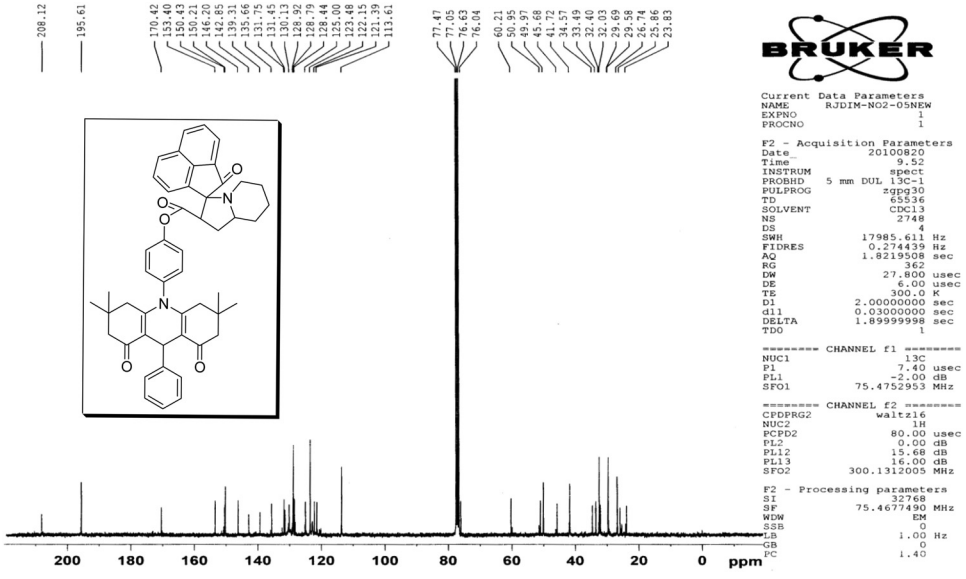

Figure A6: [13]C NMR spectrum of compound **13a**.

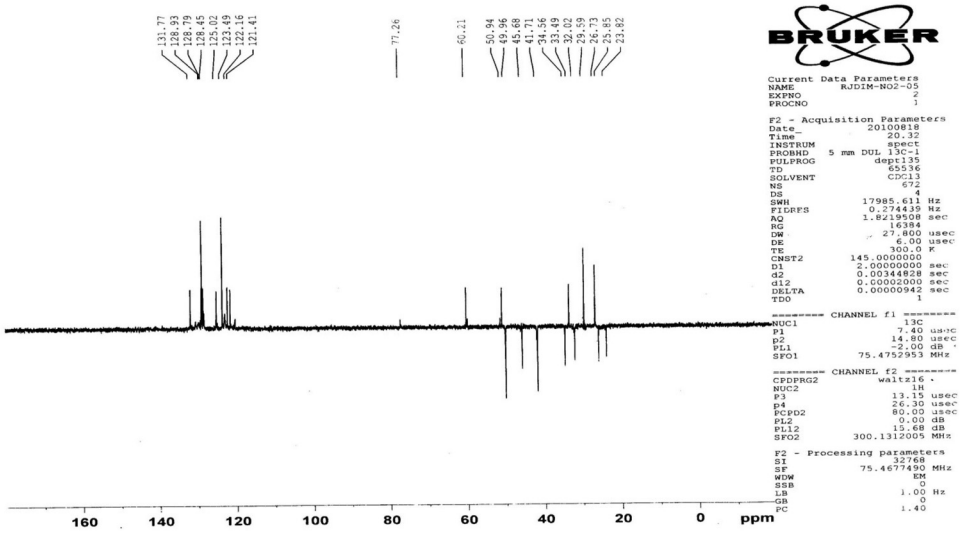

Figure A7: DEPT 135 NMR spectrum of compound **13a**.